

# Heterarchical modelling of comminution for rotary mills: Part I – Particle crushing along streamlines

**Mukesh Singh Bisht**

The University of Sydney

**François Guillard**

The University of Sydney

**Paul Shelley**

Molycop Innovation

**Benjy Marks**

The University of Sydney

**Itai Einav** (✉ [itai.einav@sydney.edu.au](mailto:itai.einav@sydney.edu.au))

The University of Sydney

---

## Research Article

**Keywords:** Hierarchy, Comminution, Particle size distribution, Streamlines, Granular flows, AG mill, rotary mill

**Posted Date:** February 15th, 2024

**DOI:** <https://doi.org/10.21203/rs.3.rs-3938200/v1>

**License:**  This work is licensed under a Creative Commons Attribution 4.0 International License.

[Read Full License](#)

**Additional Declarations:** No competing interests reported.

---

# Heterarchical modelling of comminution for rotary mills: Part I — Particle crushing along streamlines

Mukesh Singh Bisht<sup>1,2</sup>, François Guillard<sup>1</sup>, Paul Shelley<sup>2</sup>, Beny Marks<sup>1</sup>,  
Itai Einav<sup>1\*</sup>

<sup>1</sup>School of Civil Engineering, The University of Sydney, Sydney, 2006, NSW, Australia.

<sup>2</sup>Molycop Innovation, Molycop, Omaha, 68106, Nebraska, USA.

\*Corresponding author(s). E-mail(s): [itai.einav@sydney.edu.au](mailto:itai.einav@sydney.edu.au);

## Abstract

Rotary mills aim to effectively reduce the size of particles through a process called comminution. Modelling comminution in rotary mills is a challenging task due to substantial material deformation and the intricate interplay of particle kinematics of segregation, mixing, crushing, and abrasion. Existing particle-based simulations tend to provide predictions that cannot cope with the large number of particles within rotary mills, their wide range of sizes, and the physics dictating the crushing of individual particles. Similarly, there is currently no deterministic modelling means to determine the evolving population of particle sizes at any point in time and space within the mill. The aim of this two-part contribution is to address these gaps by advancing a framework for a novel stochastic comminution model for rotary mills, which has a well-defined deterministic continuum limit and can cope with arbitrarily large numbers of particles. This work describes the basic physics and structure of the new model within a heterarchical framework for ball and autogenous grinding mills. The primary focus of this Part I paper is to develop a computational model for the integration of motion of material along streamlines inside a mill. Coupled to this process is the kinetic physics dictating particle crushing. In a subsequent work, Part II, segregation and mixing will be added to this model such that realistic behaviour from the mill can be observed.

**Keywords:** Hierarchy, Comminution, Particle size distribution, Streamlines, Granular flows, AG mill, rotary mill

## 1 Introduction

Comminution is the process of reducing the size of particles, which in the mineral processing is achieved using different machinery such as crushers, rotary mills, vertical mills, and high pressure grinding rolls. These crucial unit operations are overwhelmingly energy intensive. The mineral processing industry is estimated to consume 3-4% of global energy [27, 36], where nearly half of that energy is spent in the milling operation [58, 26,

57, 6]. Here, our focus is on the rotary mills. Currently, there is no deterministic model that can explain the particle size dynamics within these mills. In this study, we introduce a novel approach based on the multiscale heterarchical modelling paradigm [40] to unveil the particle size dynamics within these mills.

The most common statistical approach to model comminution is the population balance model (PBM) [43, 11, 65, 12]. However, the major drawback of these models is that they treat the

22 particles irrespective of their position in the mill,  
23 with the mill acting essentially as a black box.  
24 The purpose of PBM models is to track the dis-  
25 tribution of sizes of all the particles in the mill,  
26 irrespective that at any point within it that dis-  
27 tribution actually varies strongly. Ignoring this  
28 fact, the performance of PBM models hinges upon  
29 the empirical calibration of global breakage and  
30 selection functions. The calibration is typically  
31 made for a given set of operating parameters by  
32 curve fitting the results against the observed prod-  
33 uct size distribution, when available. Beyond the  
34 range used for their original calibration, these  
35 models tend to fail, and cannot provide sufficient  
36 insights. This is because they are not informed by  
37 either the geometry of the mill or the composition  
38 of the material. As such they cannot say much  
39 about the role of physical entities, such as the  
40 sizes of the grinding balls, the widths of the lifters,  
41 the opening of the grates from which the material  
42 flows, or the mineralogy of the particles. In sum-  
43 mary, while PBM models may provide a first step  
44 into the problem, they cannot be used with con-  
45 fidence, especially when it comes to the potential  
46 optimisation of the performance of mills in terms  
47 of their vast energy consumption and wear.

48 Unlike PBM, in recent years the discrete ele-  
49 ment method (DEM) has been introduced to  
50 model comminution in a way that attempts to  
51 track individual particle motions and their sequen-  
52 tial crushing [14, 16, 61, 17]. One of the prob-  
53 lems with DEM models is that they are overly  
54 expensive computationally, and thus they cannot  
55 actually track all the many particles rotating in  
56 a typical mill. For example, considering a typical  
57 product size distribution in industrial autogenous  
58 grinding (AG) mills [10] with sizes ranging from  
59 10  $\mu\text{m}$  to  $\sim 100$  mm, the number of particles in the  
60 mill may be estimated to be over  $10^{14}$ . Nowadays,  
61 even the most advanced DEM models supported  
62 by high-performance computers may only track  
63 up to  $\sim 10^6$  particles over the long typical life-  
64 times of minerals within the mill. This means  
65 that DEM models can only handle  $\sim 10^8$  times  
66 fewer particles than reality. While such models  
67 can still provide excellent information regarding  
68 the bulk kinematics of the particles and the typ-  
69 ical bulk stresses that develop within the mills,  
70 they cannot be used to predict the real liber-  
71 ated particle surfaces during the process, which  
72 controls the energetic performance of the mill.

73 With particle surface area scaling quadratically  
74 with particle size, DEM models may only liber-  
75 ate  $\sim 10^{16}$  times less actual fracture surface than  
76 those liberated within real mills. In a related way,  
77 the fracture criteria implemented in DEM models  
78 tend to grossly simplify the intricate sub-particle  
79 processes that drive the crushing of individual par-  
80 ticles, as the surfaces of the fragments created are  
81 substantially limited. Another problem with DEM  
82 models, which is linked to their high computa-  
83 tional cost, is that unlike PBM models they tend  
84 to provide noisy predictions, which often over-  
85 whelm qualitative trends that modellers attempt  
86 to portray. In short, while aiming to resolve the  
87 shortcomings of PBM models in tracking physical  
88 processes, DEM models generate noisy results and  
89 fail to generate anywhere close to the amount of  
90 surfaces and fragments created in real mills.

91 In an attempt to resolve the noisiness issue  
92 of DEM models, research in geomechanics has  
93 introduced hierarchical multiscale models, which  
94 can theoretically track the distribution of parti-  
95 cles. In particular, the finite element method and  
96 the discrete element method (FEM-DEM) [4, 46,  
97 32] have been coupled, whereby DEM simulation  
98 replaces the constitutive model at the Gauss point  
99 in an FEM simulation. This multiscale model is  
100 hierarchical in nature, as it couples two differ-  
101 ent models for two distinguishable scales – the  
102 DEM operating at the particle scale, and the FEM  
103 at the continuum engineering scale. As described  
104 in [40], hierarchical multiscale FEM-DEM mod-  
105 els may only capture particle size dynamics in  
106 closed systems, which do not involve segreg-  
107 ation and mixing between the Gauss points [38, 66, 59].  
108 However, for open systems such as grinding mills,  
109 the particles continuously advect and swap places  
110 through mixing and segregation. This preferential  
111 motion by size and density prevents hierarchi-  
112 cal multiscale models from predicting particle size  
113 dynamics in grinding mills. When the particles  
114 move and deform, using these hierarchical multi-  
115 scale models essentially means we need to transfer  
116 information (*i.e.*, particle size in this context)  
117 from one Gauss point to another in the finite ele-  
118 ment simulation, which is not feasible due to the  
119 separation of scales in their structure.

120 Here we resolve the practical issues of using  
121 DEM and PBM for rotary mills by advancing an  
122 alternative multiscale approach, which unlike hier-  
123 archical DEM-FEM models is heterarchical. To

124 this end, we follow the original ideas advanced 175  
 125 by [40] to simultaneously describe the mechanisms 176  
 126 of crushing, mixing, and segregation of particles. 177  
 127 Just like PBM models, the heterarchical model 178  
 128 is capable of accommodating an arbitrarily large 179  
 129 number of particles. However, unlike PBM mod- 180  
 130 els, the heterarchical approach can further provide 181  
 131 information regarding the particle size distribu- 182  
 132 tions at any point in time and space within the 183  
 133 rotary mill domains. This new approach follows 184  
 134 a stochastic structure with a well-defined contin- 185  
 135 uum limit for open system particle size dynamics 186  
 136 such as segregation and mixing [40] and closed 187  
 137 system ones such as crushing [33]. This multiscale 188  
 138 approach is an alternative to the other hierarchi- 189  
 139 cal multiscale approaches as here there is no scale 190  
 140 separation between the representative volume and 191  
 141 the continuum scale, both scales coexist within 192  
 142 a single framework. This facilitates the transfer 193  
 143 of information (*i.e.*, particle size) from one scale 194  
 144 to another as well as within the representative 195  
 145 volume scale. Nevertheless, so far heterarchical 196  
 146 models were limited to simple flow systems that 197  
 147 may be idealised using only one spatial coordi- 198  
 148 nate, such as those occurring during the granular 199  
 149 avalanches, landslides, and debris flows [7, 50, 23, 200  
 150 51]. Furthermore, thus far the description of crush- 201  
 151 ing in the framework ignored the role of kinetic  
 152 particle collisions, dealing solely with quasi-static  
 153 comminution.

154 In this study, we extend the heterarchical 202  
 155 framework to track comminution in higher spa- 203  
 156 tial dimensions. For the first time, the approach 204  
 157 is used to model comminution in rotary mills. To 205  
 158 deliver these goals the heterarchical approach is 206  
 159 here coupled with the streamline method, origi- 207  
 160 nally called the strain path method in [5], which 208  
 161 has been used in the past to integrate constitutive 209  
 162 laws for predicting penetration resistance [24] in 210  
 163 geomechanics. Here, rather than integrating con- 211  
 164 stitutive models, the streamline method would be 212  
 165 used to integrate the heterarchical method.

166 In summary, the current two-part study offers 213  
 167 three significant novel contributions. Firstly, we 214  
 168 extend the crushing model within the heterar- 215  
 169 chical approach to account for kinetic crushing, 216  
 170 which goes beyond quasi-static conditions in pre- 217  
 171 vious publications. This factor is shown to be 218  
 172 particularly important for rotary mills, where the 219  
 173 particles are often advected through highly turbu- 220  
 174 lent regions. Secondly, we integrate the heterarchy 221  
 175

176 and the streamline methods to investigate the pro- 177  
 176 gression of comminution in rotary mills. Lastly, by 178  
 177 tessellating the material domain within the mill 179  
 178 for equal mass material points along streamlines, 180  
 179 the new streamline-heterarchical method enables 181  
 180 us to model mixing and segregation in rotary 182  
 181 mills. These contributions collectively advance the 182  
 183 understanding of comminution processes and offer 184  
 184 new insights into the intricate dynamics occurring 185  
 185 in rotary mills.

186 This is the first paper of a two-part series. 187  
 187 Here, we present the application of heterarchy in 188  
 188 rotary mills for two cases: a ball mill and an AG 189  
 189 mill. In this Part I, we discuss comminution by 190  
 190 solely considering the mechanism of crushing. The 191  
 191 other two important mechanisms of mixing and 192  
 192 segregation will be addressed in Part II. The cur- 193  
 193 rent paper is organised as follows: We begin by 194  
 194 explaining the heterarchical model for quasi-static 195  
 195 comminution and its extension to kinetic comminution. 196  
 196 Next, we synthesise the kinematics of 197  
 197 granular flow in rotary mills, as an essential step 198  
 198 for the streamline method. Finally, we discuss the 199  
 199 implementation of heterarchy along streamlines in 200  
 200 rotary mills.

## 2 Heterarchical model for comminution

201 This section starts with a brief introduction to 202  
 202 the basic concepts of the heterarchical model [40] 203  
 203 for quasi-static comminution, with a focus on par- 204  
 204 ticle crushing. The capacity of the framework to 205  
 205 handle further crushing in dynamic settings is 206  
 206 then extended by allowing for kinetic comminution, 207  
 207 which is expected to develop in rotary mills 208  
 208 due to frequent particle collisions.

209 In the heterarchical framework, the physical 210  
 210 system of a polydisperse granular medium is dis- 211  
 211 cretized into a number of representative volume 212  
 212 elements (RVEs) each containing a statistically 213  
 213 significant number of particles as illustrated for 214  
 214 a one-dimensional column of particles in Fig. 1. 215  
 215 The particles within each RVE are further mapped 216  
 216 into an array of  $M$  number of cells. The inter- 217  
 217 nal coordinate, along which the volume within a 218  
 218 RVE is discretized, is called the micro-structural 219  
 219 coordinate and it is such that the position along 220  
 220 this coordinate represents the local neighbour- 221  
 221 hood of particles. The model can be defined in 222  
 222

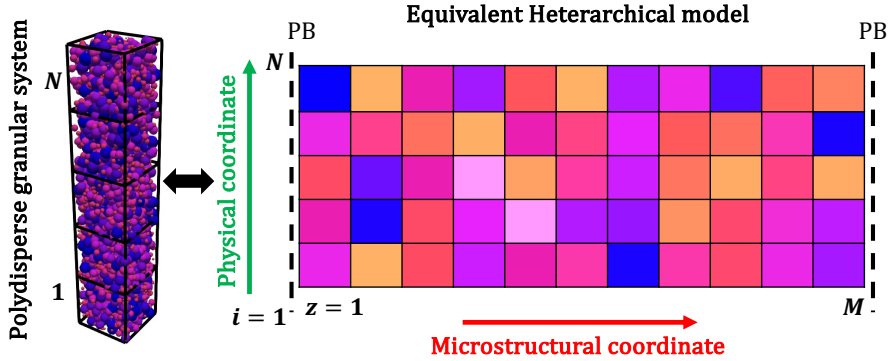


**Fig. 1:** Illustrative example for the structure of a heterarchical model. On the *Left*, a physical one-dimensional polydisperse granular system. On the *Right*, an equivalent heterarchical model. The physical granular system is discretized into a number of representative volume elements (RVEs) along the physical coordinate. The particles within each RVE are then further mapped along the micro-structural coordinate into an array of particle sizes  $s_i^t = (s_{i,1}^t, s_{i,2}^t, \dots, s_{i,M}^t)$  at time  $t$  with periodic boundary (PB) conditions (colour figure online).

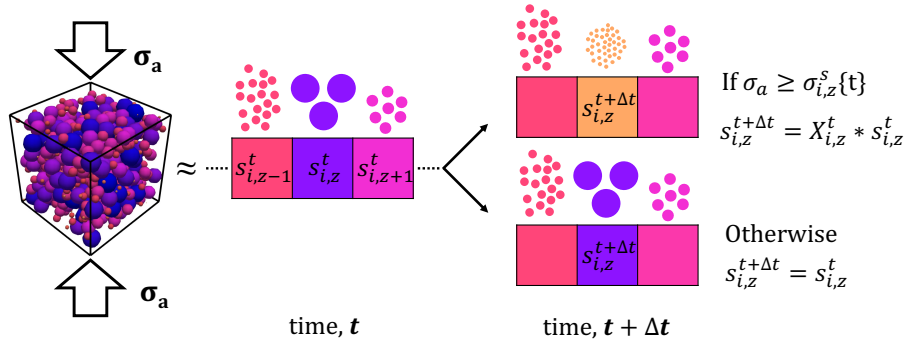


**Fig. 2:** The stochastic comminution rule of the heterarchical model for a cell  $(i, z)$  under externally applied stress  $\sigma_a$ . At any given time  $t$ , if the external stress acting on the particles ( $\sigma_a$ ) is greater than or equal to the crushing strength ( $\sigma_{i,z}^s$ ) of particles, the particle size in that cell is reduced by a factor  $X_{i,z}^t$  in the next time step  $t + \Delta t$ . Otherwise, the particle size remains unchanged (colour figure online).

a lattice in any number of spatial (external) and micro-structural (internal) dimensions. The spatial and micro-structural coordinates together form a higher dimensional framework such that each coordinate is orthogonal to one another.

In Fig. 1 the first index ( $i$ ) represents the spatial coordinate of the position of the RVE and the second index ( $z \in [1, M]$ ) represents the micro-structural coordinate along which the RVE is discretized. Furthermore, the system is deemed periodic along the heterarchical coordinate  $z$ . The

number of cells ( $M$ ) along the heterarchical coordinate ( $z$ ) should be sufficiently large so that upon averaging it gives a smooth particle size distribution (PSD) for a RVE. Each cell contains particles of uniform size and the total mass of particles in a cell remains constant even though the particle size of a cell may evolve. This may be due to crushing, as detailed in this Part I of the paper, as well as by mixing and segregation, as explained and assessed later in Part II. Moreover, the heterarchical model considers that the crushing of

245 particles in a cell is dependent not only on the  
 246 properties of the particles in the cell, but also  
 247 on those in their neighbouring cells. Therefore,  
 248 at any instant a given cell has to consider the  
 249 information of its neighbouring cells (immediate  
 250 neighbours). For cells 1 and  $M$ , *i.e.*, first and last  
 251 cells, the immediate neighbouring cells are  $(M, 2)$   
 252 and  $(M - 1, 1)$ , respectively, owing to the periodic  
 253 boundary condition.

## 254 2.1 Quasi-static comminution

To model comminution we need to define the conditions for the onset of particle crushing and the fragment size distribution for crushed particles. The onset of crushing occurs at any time  $t$  when the externally applied (bulk) stress ( $\sigma_a$ ) is greater than or equal to the crushing strength ( $\sigma_{i,z}^s(t)$ ) of the particles. If this criteria is met, at the next time step  $t + \Delta t$ , the particle size at cell location  $(i, z)$  is reduced by some factor. Otherwise, the particle size in that cell is kept unchanged (see Fig. 2). The above comminution rules are applied to each cell of the RVE, and each cell of the RVE is subjected to the same external applied stress ( $\sigma_a$ ). Accordingly, the particle size of the  $(i, z)^{th}$  cell evolves as

$$288 s_{i,z}^{t+\Delta t} = \begin{cases} X_{i,z}^t s_{i,z}^t & \text{if } \sigma_a \geq \sigma_{i,z}^s(t) \\ 289 s_{i,z}^t & \text{otherwise,} \end{cases} \quad (1)$$

255 where  $X_{i,z}^t$  is the factor determining how much  
 256 the size is reduced, and is a random variable  
 257 between 0 and 1 drawn from the fragment size  
 258 distribution. Commonly used fragment size  
 259 distributions include the Weibull and power law  
 260 distributions [13, 19, 48, 52]. Here, the distribu-  
 261 tion is based on Weibull's two-parameter model  
 262 as described in [40]. We also impose the condi-  
 263 tion on the minimum size of the fragment ( $s_{min}$ )  
 264 generated, which in this study has been set to  
 265  $s_{min} = 1 \mu\text{m}$ . Therefore, the probability density  
 266 function of the fragment size distribution  $f(x)$   
 267 over  $x \in (x_m, 1]$  is given as

$$268 f(x) = \frac{\frac{k}{\lambda} \left( \frac{x-x_m}{\lambda} \right)^{k-1} \exp\left[-\left(\frac{x-x_m}{\lambda}\right)^k\right]}{1-\exp\left[-\left(\frac{1-x_m}{\lambda}\right)^k\right]}, \quad (2)$$

269 where  $x_m = s_{min}/s$ . The parameters  $k$  and  $\lambda$  can  
 270 be determined experimentally for the fragment  
 271 size distribution of any given mineral particle [64].

In the original work by Marks & Einav [40], for the  $z^{th}$  cell of the  $i^{th}$  RVE, the crushing strength of particles under quasi-static conditions was expressed as

$$\sigma_{i,z}^s(\vec{s}) = \sigma^m \left( \frac{s_{i,z}}{s^m} \right)^{-3/w_s} \exp \left[ \frac{\log^2(s_{i,z}/\bar{s}_{i,z})}{2n^2} \right], \quad (3)$$

271 where  $\vec{s} = \{s_{i,z-1}, s_{i,z}, s_{i,z+1}\}$  represents the parti-  
 272 cle size in the considered cell as well as its nearby  
 273 neighbours;  $\sigma^m$  the crushing strength of parti-  
 274 cle corresponding to the maximum particle size  
 275  $s^m$  in the system;  $\bar{s}_{i,z} = (s_{i,z-1} + s_{i,z+1})/2$  the  
 276 average local neighbourhood particle size;  $w_s$  the  
 277 Weibull modulus for strength; and  $n$  is a non-  
 278 dimensional scaling constant as described by [40].  
 279 In the above equation, the second term (power law  
 280 term) accounts for the effect of particle size on  
 281 the crushing strength primarily due to the pres-  
 282 ence of internal flaws within the particles [41]. The  
 283 third term (exponential term) accounts for the  
 284 cushioning effect on that strength [8, 40], where  
 285 smaller particles tend to shield bigger particles  
 286 from crushing.

## 2.2 Kinetic comminution

The previous section describes the crushing of par-  
 287 ticles subjected to external loading under quasi-  
 288 static loading conditions. However, in certain sce-  
 289 narios, such as in industrial mills or during rapid  
 290 granular avalanches, the particles frequently col-  
 291 lide with each other. These collisions promote  
 292 further crushing due to higher impact velocities,  
 293 which can happen even when the external pressure  
 294 acting on them is relatively small. Fig. 3 depicts  
 295 such a collision between two particles, which  
 296 results in their crushing into smaller fragments.

Considering an assembly of jiggling particles, the effect of the collisions on the crushing strength under dynamic conditions ( $\sigma_{i,z}^d$ ) could be related to the (measurable [39]) mean fluctuating velocity ( $v'$ ), which represents the typical difference between particle velocities and their ensemble average at any particular point in space and time:

$$\sigma_{i,z}^d(\vec{s}, v') = \sigma_{i,z}^s(\vec{s}) \cdot \mathcal{K}(v', s_{i,z}), \quad (4)$$

297 where,  $\sigma_{i,z}^s$  is the crushing strength of particles  
 298 under quasi-static loading as specified by Eq. 3,  
 299

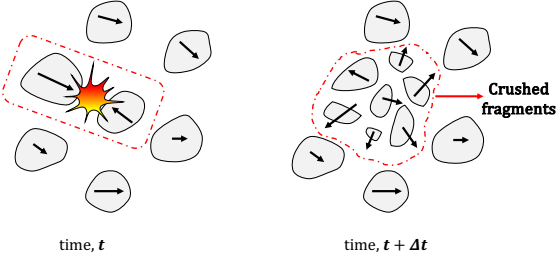


**Fig. 3:** Schematic representation of kinetic crushing of particles during high deformations. Each particle experiences an independent velocity that fluctuates from the local mean velocity field, as depicted by arrows over the particles. The particles inside the highlighted box (*left*) have a higher relative velocity at time  $t$ , which may result in crushing. The figure on the *right* shows the crushed state of the particles at time  $t + \Delta t$ . The length of the arrow (not to scale) represents the magnitude of the velocity of the particles.

301 while  $\mathcal{K}$  is introduced as a kinetic strength reduction  
302 factor that is here taken to depend on the  
303 fluctuating velocity  $v'$  and the particle size  $s_{i,z}$ .

To determine this kinetic strength reduction factor one may consider the vast experimental observations [30, 53, 54], which show that the survival probability of the particles against crushing depends on their impact velocity. With the Weibull distribution [62] being a popular and successful representation of this survival probability, the kinetic strength reduction factor is here taken to follow the same statistics

$$\mathcal{K}(v', s_{i,z}) = \exp [-(v'/v'_{50})^{w_v}], \quad (5)$$

where,  $v'_{50} = v'_{50}(s_{i,z})$  is the fluctuating velocity of a particle of size  $s_{i,z}$  corresponding to 50% survival probability against crushing, and  $w_v$  is the Weibull modulus for velocity. Both of these parameters ( $v'_{50}$  and  $w_v$ ) can be determined experimentally for a given mineral. Importantly, the work in [54] showed that  $v'_{50}$  is also a function of the particle size (here  $s_{i,z}$ ) and can be calculated as

$$v'_{50}(s_{i,z}) = a_v \exp (-b_v s_{i,z}/s_r), \quad (6)$$

304 where  $a_v$  and  $b_v$  are correlation parameters and  $s_r$   
305 is a reference particle size which in this case has  
306 been taken as equal to the maximum particle size,  
307 *i.e.*  $s_r = s^m$ .

Finally, notice that  $v'$  represents the magnitude of the velocity fluctuations, and thus can only be positive. Therefore, it is important to furthermore consider the typical direction of the fluctuations, since during expansion particles tend to move apart, so we would not expect collisions and associated crushing. Provided with the field of velocities ( $v$ ) in the rotary mill, one can calculate the volumetric strain rate from  $\dot{\varepsilon}_v = -\nabla \cdot \vec{v}$  to determine whether the medium expands or contracts. With that in mind, the particle size of a heterarchical cell in the general heterarchical comminution model for rate dependent, dynamic loading evolves according to the modified crushing criteria below

$$s_{i,z}^{t+\Delta t} = \begin{cases} X_{i,z}^t s_{i,z}^t & \text{if } \sigma_a \cdot \mathcal{H}(\dot{\varepsilon}_v) \geq \sigma_{i,z}^d(t) \\ s_{i,z}^t & \text{otherwise,} \end{cases} \quad (7)$$

308 where,  $\mathcal{H}$  is the Heaviside step function, (*i.e.* during  
309 volumetric expansion  $\dot{\varepsilon}_v < 0$  and  $\mathcal{H}(\dot{\varepsilon}_v) = 0$ , so  
310 the particles do not crush, otherwise  $\mathcal{H}(\dot{\varepsilon}_v) = 1$ , so  
311 they may crush).

### 3 Continuum fields

312 As shown in the previous section, the crushing  
313 of particles within rotary mills depends on local  
314 continuum information regarding kinematic entities  
315 such as the velocities and strain rates, as well  
316 as stress variables. Therefore, in the following, we  
317 describe how these fields could be obtained for the  
318 granular material within rotary mills.  
319

320 The methodology in this paper will follow a  
321 one-way coupling scheme. Specifically, the use of  
322 the kinematic and stress fields will be based on  
323 either analytical or numerical proxies for the flow  
324 of non-crushable particles. This has certain lim-  
325 itations since the fields retrieved ignore the fact  
326 that the particles actually crush in those mills.  
327 The tacit assumption here is that crushing would  
328 not substantially affect the measured continuum  
329 velocity and stress fields. In other words, for sim-  
330 plicity, the fields determined below are decoupled  
331 from the crushing that happens in the mill. How-  
332 ever, the extent of crushing that will be modelled  
333 later is determined based on those fields. In real-  
334 ity, we might expect some consolidation of the  
335 pack within the mill, with additional effects poten-  
336 tially arising due to frictional lubrication by the

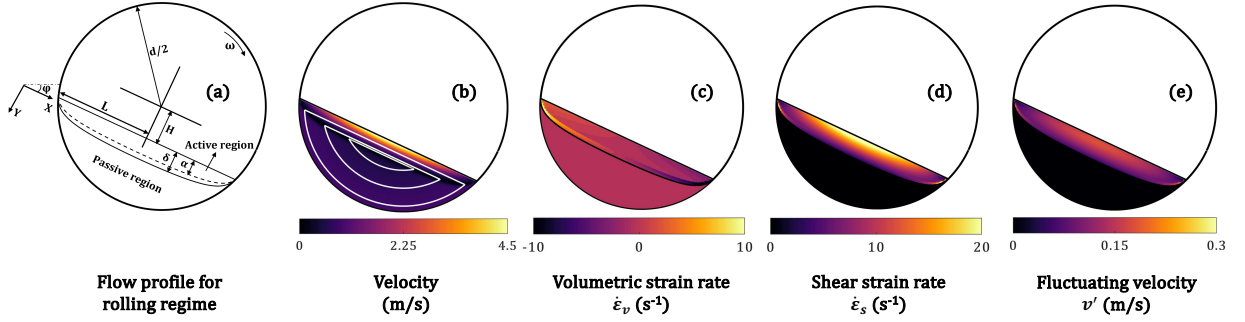


**Fig. 4:** Kinematics for a ball mill using the analytical solution by Ding et al. [22]. (a) Flow profile for the rolling regime in a ball mill. Contour plots: (b) Velocity magnitude (streamlines superimposed in white colour), (c) Volumetric strain rate (positive in compression), (d) Shear strain rate, and (e) Fluctuating velocity (colour figure online).

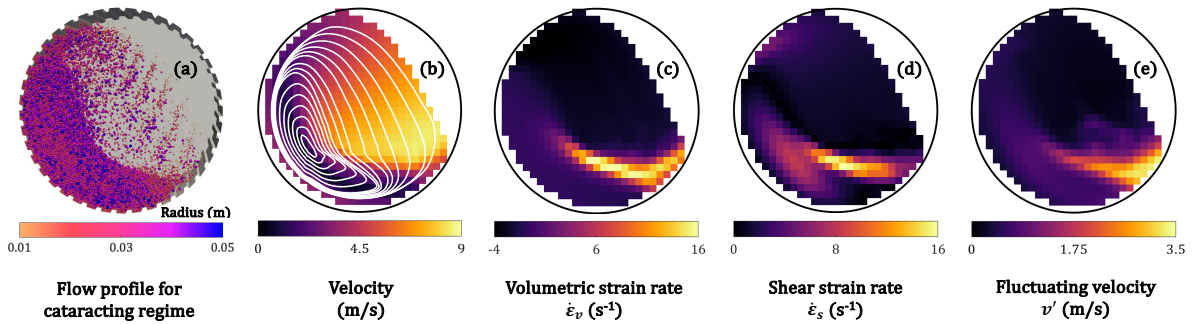


**Fig. 5:** Coarse-grained kinematics from DEM for an autogenous mill (AG). (a) Snapshot of particle distribution and their sizes for the cataracting regime in an AG mill. Contour plots: (b) Velocity magnitude (streamlines superimposed in white colour), (c) Volumetric strain rate (positive in compression), (d) Shear strain rate, and (e) Fluctuating velocity (colour figure online).

337 small fragments produced, which might alter their 354 rheological behaviour and impact the adopted 355 fields. However, these effects are here considered 356 negligible for all practical purposes. 357

341 The kinematics of the bulk material flow 358 within rotary mills can be estimated through 359 a variety of methods, including experimental, 360 numerical, or analytical calculations. Experimentally, 361 this may include imaging techniques such 362 as particle image velocimetry [35], positron emis- 363 sion particle tracking [49], and radioactive particle 364 tracking [3]. Numerically, the kinematic fields 365 could be evaluated using the discrete element 366 method (DEM), or using large-deformation finite 367 element simulations [47, 55] equipped with constitu- 368 tive granular rheology models [29]. Analytically, 369 the bulk velocity of the particles inside the mills

are often established by considering the aforementioned experimental and numerical observations, with additional input from either engineering intuition or fundamental imposition of continuum compatibility requirements [3, 22].

For demonstration purposes, the current study will explore the use of kinematics from both analytic and numerical sources. Specifically, we will demonstrate the use of the analytical velocity solution by Ding et al. [22] for ball mills and the use of a numerical velocity field for the case of an AG mill.

### 3.1 Ball mill

The details of the analytical solution for the ball mill are discussed in the Appendix. A. Ball mills are typically operated at a low rotational speed

370 where the Froude number  $F_r$  which is defined as  
 371 the ratio of centrifugal force to gravity, falls within  
 372 the range of  $10^{-4} < F_r < 10^{-2}$  [42]. Under such a  
 373 rotational speed, the bulk of the material predom-  
 374 inantly rotates as a rigid body. As the material  
 375 reaches its dynamic angle of repose, it rolls down  
 376 along the surface. The flowing layer is very thin  
 377 as compared to the pseudo-rigidly rotating bulk  
 378 (see Fig. 4a). The velocity varies linearly along  
 379 the depth of this flowing layer with a maximal  
 380 speed achieved at the free surface. Additionally,  
 381 the velocity also varies along the length of this  
 382 layer with a maximum residing at the centre of the  
 383 layer. Based on this analytical solution the velo-  
 384 city and strain rate fields for the granular flow in a  
 385 ball mill can be calculated, as shown in Figs. 4b,  
 386 4c and 4d, respectively.

Furthermore, in the case of the ball mill, the fluctuating velocity ( $v'$ ) of the particles (see Fig. 4e), as required from Section 2, can be derived as

$$v' = \sqrt{P_k/\rho_b}, \quad (8)$$

387 where  $P_k$  is the kinetic pressure and  $\rho_b$  is the bulk  
 388 density.

The kinetic pressure can be estimated for  
 395 shear-induced flow in terms of the dimensionless  
 396 kinetic number ( $I_k$ ), as introduced by [2], which  
 397 can be expressed as  $P_k = P_s I_k$ , with  $P_s$  being the  
 398 static pressure. The calculation of bulk stresses  
 399 acting on particles is discussed in the following  
 400 subsection. Furthermore, the kinetic number can  
 401 be approximated from [2] as  $I_k = I$ , where  $I =$   
 402  $\dot{\varepsilon}_s \bar{s} \sqrt{\rho_m/P}$  is the inertial number [20],  $\dot{\varepsilon}_s$  the shear  
 403 strain rate,  $\bar{s}$  the mean particle size,  $\rho_m$  the mate-  
 404 rial density, and  $P$  the total pressure (sum of  
 405 static pressure and kinetic pressure). Given these  
 406 relations, the kinetic pressure may be estimated  
 407 analytically from:

$$P_k = \dot{\varepsilon}_s \bar{s} \sqrt{\rho_m P}. \quad (9)$$

Finally, the bulk static pressure ( $P_s$ ) is  
 413 assumed to be a linear function of depth ( $y \cos \varphi$ )  
 414 measured from the free surface, i.e.  
 415

$$P_s = \rho_b g y \cos \varphi, \quad (10)$$

389 where  $\rho_b$  is the bulk density,  $g$  is the acceleration  
 390 due to gravity and  $\varphi$  is the dynamic angle of repose  
 391 of material. The calculation of bulk density will  
 421

be discussed in Section 4.3. The modelled static  
 392 pressure field for the ball mill is shown in Fig. 6a.  
 393

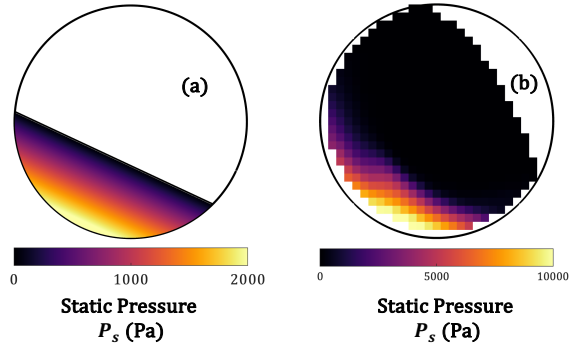


Fig. 6: Static pressure field for (a) Ball mill using Eq. 10, and (b) AG mill using coarse-graining (see Appendix. B) from DEM simulation (colour figure online).

### 3.2 AG mill

The numerical simulations from which we retrieve  
 395 the above quantities for the AG mill are based on  
 396 a standard DEM model, whose technical details  
 397 are provided and discussed in Appendix. B. The  
 398 DEM simulations have been used to extract the  
 399 required continuum field variables using coarse-  
 400 graining [28, 63] for the AG mill case. These con-  
 401 tinuum fields are consistent with previous results  
 402 by others for rotary mills [12, 16, 17]. In this case,  
 403 the mill is operated at a high rotational speed  
 404 ( $0.1 < F_r < 1$ ) [42] such that we generally observe  
 405 a cataracting flow [42, 16, 18] which is character-  
 406 ized by the individual particles detaching from the  
 407 bed and being thrown off into free space inside the  
 408 mill as shown in Fig. 5a. The obtained continuum  
 409 velocity, strain rate, and fluctuating velocity fields  
 410 from the DEM simulation are shown in Figs. 5b,  
 411 5c, 5d and 5e, respectively.

In addition to information on the kinematics  
 413 of the particles, we also need to have informa-  
 414 tion about the static stresses acting on them at  
 415 any point in space and time inside the mill. For  
 416 the case of the AG mill, the corresponding static  
 417 pressure field is extracted from the DEM simula-  
 418 tion using coarse-graining, as described again in  
 419 Appendix. B. The static pressure field for the AG  
 420 mill is shown in Fig. 6b.

## 4 Integrating heterarchy along the streamlines

The preceding sections described the essential components of our comminution model, *i.e.*, the heterarchical model of kinetic crushing of particles and the kinematics of the particles within rotary mills. In this section, we delve into the implementation of the heterarchical model for the rotary mills, marking the second novel contribution of this study.

The concept of heterarchy is extended to the rotary mills by leveraging the potential of the streamline method, previously known in geomechanics as the strain path method [5]. Specifically, past work by [24] had demonstrated the effectiveness of the streamline method by integrating advanced constitutive assumptions along streamlines to determine the penetration resistance of natural soils subjected to large deformations. Rather than integrating constitutive assumptions, the novelty here is in integrating instead the heterarchical model along the streamlines to form a new powerful tool with which we could investigate the evolution of the particle size distributions at any point in time and space within the rotary mills.

### 4.1 Streamlines

Using the velocity fields in Section 3 for both the ball and the AG mills, the first step is to obtain a corresponding set of streamlines. As described earlier, the flow is assumed to follow steady state kinematics, and thus the streamlines should form a closed loop in order to allow the material to flow continuously along them as the mill rotates. The following section explains our methodology for obtaining these closed sets of streamlines, which play a crucial role in the new comminution model.

#### 4.1.1 Ball mill

The streamlines in the ball mill are established by considering the velocity fields in both the active and passive regions of the flow (see Appendix A). In the active region, the velocities are distributed linearly along the depth of flow in the streamwise direction (X-axis) and the velocity along the other direction (Y-axis) is negligible. Consequently, the particles can be assumed to move in a linear path within the active region, from which

we define in that region a set of streamlines parallel to the X-axis, with their endpoints lying on the zero-velocity ( $\alpha$ ) line.

In the passive region, the particles move along the drum as a rigid body, allowing us to define the streamlines as circular arcs, with their endpoints positioned at the interface of the active and passive regions ( $\delta$ -line). To ensure that the streamlines form closed loops, the streamlines are assumed to follow circular arcs between the active-passive interface ( $\delta$ ) and the zero-velocity ( $\alpha$ ) line, as defined in Appendix A. This approach indeed produces closed streamlines, as illustrated in Fig. 7a.

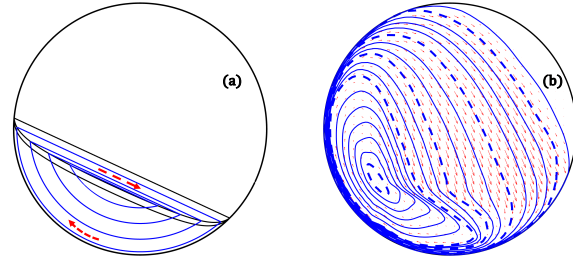


**Fig. 7:** Streamlines in: (a) the ball mill obtained using the analytical velocity solution by Ding et al. [22], and (b) the AG mill obtained using Spline interpolation from the coarse-grained DEM velocity field. The streamlines are superimposed over the velocity vector data (shown in red colour) from DEM. The streamlines represented by dotted lines are the *master streamlines*, while the rest are interpolated using them. The number of streamlines in panels (a) and (b) are just for visualisation, while in the actual simulations the number of streamlines is much higher.

Notice, however, that the consequence of the analytic solution is that we must introduce a velocity component in the Y-direction for the portion of the streamlines between the  $\delta$ -line and the  $\alpha$ -line. This addition is necessary to enable the material to flow along the circular curve since the particles initially possess velocity solely in the X-direction within this region.

#### 4.1.2 AG mill

The scheme for constructing closed streamlines for the AG mill is different since the kinematics

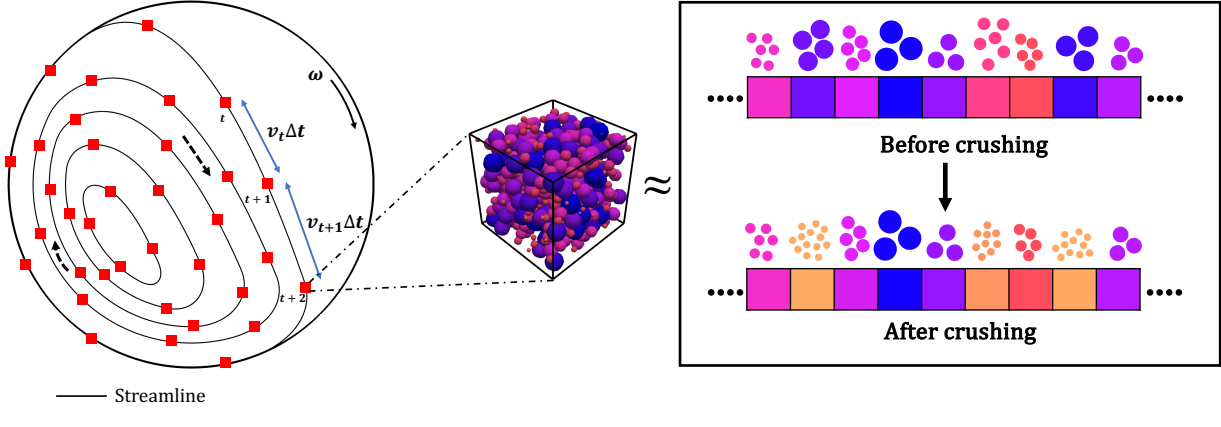


**Fig. 8:** Schematic allocation of material points along streamlines for the flow within an example rotary mill. The material points are distributed by marching along the length of the streamlines in discrete time-step  $\Delta t$ . The material points shown here are just for visualisation, while in the actual simulations they are distributed by adopting a very small time step. The granular mass within a material point is then further discretized along the micro-structural coordinate. Such a scheme is applied to both the ball and the AG mills (colour figure online).

have been established thanks to the coarse-grained velocity field derived from the DEM simulation. Given this velocity field, the streamlines for the granular flow can be directly generated using MATLAB. However, given the inevitable numerical noise, the streamlines that are generated from MATLAB would not necessarily form the required set of closed streamlines.

To obtain closed streamlines, we adopt the following alternative approach. We start by selecting a subset of streamlines generated from MATLAB, ensuring they cover the entire flow region. In order to close these streamlines, we strategically add additional data points where needed and then generate a Spline function [25]. These carefully selected streamlines are referred to as *master* streamlines for the bulk flow within the AG mill. By employing the Spline function, we can effectively interpolate any number of streamlines between any of these *master* streamlines, as illustrated in Fig. 7b. This technique allows us to obtain a set of closed streamlines that accurately describe the granular flow inside the AG mill.

## 4.2 Material points on streamlines

Once the closed streamlines for the bulk material flow are obtained, the subsequent step is to allocate discrete set of material points on the

streamlines. Each material point is defined as a representative volume element (RVE) in space, which holds a fixed mass of particles. To achieve this, we march along the length of a streamline in discrete time-steps  $\Delta t$ , as illustrated in Fig. 8. The time-step  $\Delta t$  is chosen to be sufficiently small, ensuring that the evolution of the particle sizes within a volume element remains independent of its value. Also, the total number of streamlines considered for the bulk material flow should be sufficiently high such that the evolution of the overall particle size distribution for the whole material inside the mill is independent of the number of streamlines.

The position of a material point along the streamline at any time-step can be calculated using the Verlet integration scheme [34] as

$$X(t + \Delta t) = X(t) + v(t)\Delta t + \frac{1}{2}a(t)\Delta t^2, \quad (11)$$

where  $\Delta t$  is the time-step,  $v$  and  $a$  are the bulk velocity and acceleration, respectively, obtained from the velocity field. The term  $\frac{1}{2}a(t)\Delta t^2 \approx 0$  in Eq. 11 for very small accelerations, as long as the time-step ( $\Delta t$ ) chosen is very small. Therefore,  $X(t + \Delta t) = X(t) + v(t)\Delta t$  is also a good approximation to determine the position of a material point in subsequent time-steps. Considering the

above, it is important to make a couple of observations with respect to the distribution of the material points along the streamlines:

1. For the ball mill case, near the vicinity of the zero-velocity line ( $\alpha$ -line) the accelerations are actually significant since the velocities transform rapidly from  $v = 0$  on the  $\alpha$ -line to some non-zero value on the  $\delta$ -line, given by the analytic velocity solution. Therefore, in Eq. 11 the term  $\frac{1}{2}a(t)\Delta t^2 \neq 0$ , and does actually have a significant role. In fact, it is the acceleration that drives the material when it lies on the  $\alpha$ -line, since  $v = 0$  at that location.
2. For the AG mill case, the streamlines are obtained using Spline interpolation. It was observed that the gradient of a streamline may not always be precisely oriented along the velocity vector obtained from the DEM simulation, as depicted in Fig. 7b, where the interpolated streamlines are superimposed over the velocity vectors obtained from DEM simulation. However, while distributing the material points along the streamlines, we neglect this second-order effect and assume that the velocity vectors are parallel to the streamlines.

The positions of the material points along the streamlines remain as such and do not need to be updated further during the simulation.

### 4.3 Tessellation into subvolumes

Given a set of material points along the streamlines, the material domain within the mill is tessellated into subvolumes. To compute the sub-volume occupied by a material point in space we have used the Voronoi neighborhood method [1] as shown in Fig. 9. The volume will therefore be equal to the area of the Voronoi polygon assuming unit length along the mill axis. These Voronoi subvolumes are here required for the purpose of mass calculation, while in the following paper (Part II) they will be further required for implementing the segregation and mixing mechanisms.

Each of the Voronoi subvolumes are then further discretised along the micro-structural coordinate ( $z$ ) into  $M$  cells as shown in Fig. 8. Therefore, the whole volume of a material point is divided into  $M$  subvolumes, each containing particles of different sizes which evolve as the system undergoes crushing.

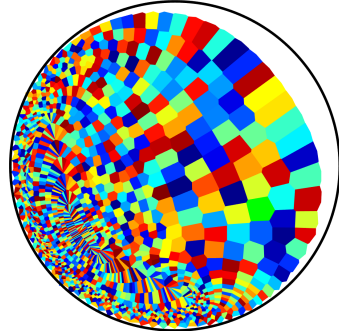


**Fig. 9:** Volume of material points for the granular flow in AG mill calculated using the area obtained from Voronoi polygons [1]. The length along the axis of the mill is assumed to be unity. The polygons are coloured randomly (colour figure online).

The mass of particles in a given material point can therefore be obtained as  $\mathcal{M} = \rho_b V$ , where  $\rho_b$  is the bulk density and  $V$  is the volume of a material point calculated using the Voronoi polygon method.

For the AG mill, the bulk density field is obtained from the DEM simulations, where the resulting spacing of the material points is determined using the associated velocity field. This purely numerical approach leads to a certain level of variation between the masses of the material points, which in theory needs to be constant. In the case of the current simulation, this variation/error is at the order of 13.8%. In the following, we consider the effects of this variation to be negligible. In the future, a correction scheme may be developed to alleviate this issue so as to ensure the constancy of the material point masses.

For the ball mill, the bulk density field is obtained by integrating the bulk density along the material points of a streamline using a suitable integrating scheme. Correspondingly, the material points are spaced using the analytical velocity field. As such, this method does in fact ensure the constancy of the material point masses. Here, using the forward Euler method, the bulk density field can be calculated as:

$$\rho_{b_{\{p,q\}}} = \rho_{b_{\{p,q-1\}}} + \rho_{b_{\{p,q-1\}}} \dot{\varepsilon}_{v\{p,q-1\}} \Delta t, \quad (12)$$

where the indices  $p \in [1, N_s]$ , and  $q \in [1, N_p]$  represent the streamline and the corresponding material point along it.  $N_s$  is the total number of

**Table 1:** Simulation parameters

Parameters	Symbol	Value		Unit
		Ball mill	AG Mill	
<b>Geometrical Parameters</b>				
Mill Diameter	$d$	0.30	6	m
Degree of filling	$f$	30	30	%
Dynamic angle of repose	$\varphi$	25°	-	degree
<b>Mechanical Parameters</b>				
Rotational velocity	$\omega$	6.3	13.5	rpm
Material density	$\rho_m$	2500	2500	$\text{kgm}^{-3}$
Scaling parameter	$n$	0.05	0.05	
Fragment size distribution parameters	$k$	4	4	
	$\lambda$	1	1	
Crushing strength (for particle size $s^m$ )	$\sigma^m$	0.5	50	kPa
Weibull modulus for strength	$w_s$	2	2	
Weibull modulus for velocity	$w_v$	6	6	
Correlation parameters for impact velocity	$a_v$	0.2	1.5	$\text{ms}^{-1}$
	$b_v$	0.4	0.4	

streamlines and  $N_p$  is the total number of material points along a given streamline.  $\dot{\varepsilon}_v$  is the volumetric strain rate and  $\Delta t$  is the time step that we chose to discretise the streamlines into discrete material points.

## 5 Simulations and results

It is now possible to demonstrate how the newly defined ‘heterarchical streamline method’ may be used to analyse the process of comminution within rotary mills. So far the method can only accommodate for the physics of kinetic particle crushing, leaving aside the treatment of further effects of segregation and mixing to the next Part II of this work. Here, we show the application of this model in predicting the particle size distribution at any point in space and time in rotary mills, for the examples of ball and AG mills using the previously defined fields.

The geometrical and mechanical parameters used for the simulations are listed in Table 1. All these parameters have a clear statistical meaning and can be determined experimentally. The crushing strength parameters ( $\sigma^m$  and  $w_s$ ) can be determined experimentally for any mineral using several single particle crushing tests [44, 45]. The impact velocity parameters ( $a_v$ ,  $b_v$  and  $w_v$ ) can also be determined experimentally for any given mineral using impact crushing tests [56, 60, 13].

Note that for this study, we use the geometrical and mechanical parameters which are typical for an industrial-scale AG mill. For the case of our conceptual ball mill, we use scaled parameters that are obtained for the AG mill, specifically the mineral strength parameters. At this stage, we have not explicitly included the grinding media in the heterarchical model, which plays a crucial role in the comminution for ball mills. We assume the crushing in the ball mill occurs only

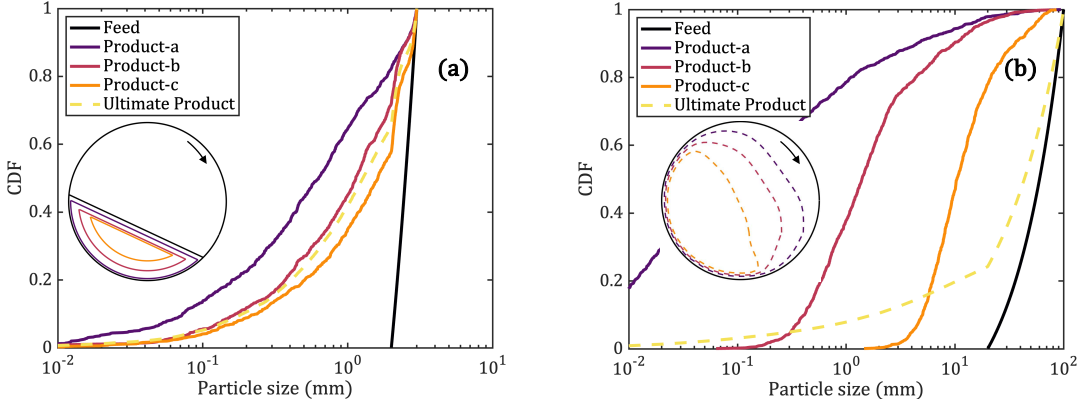


**Fig. 10:** Cumulative distribution function (CDF) of product particle sizes along different streamlines after one mill revolution. (a) Ball mill, and (b) AG mill. The insets show the actual location of the corresponding streamlines in the flow region. An ultimate product size distribution for the entire minerals within the mills is also plotted. The number of cells used along the micro-structural coordinate for each simulation are  $M = 10^3$  (colour figure online).

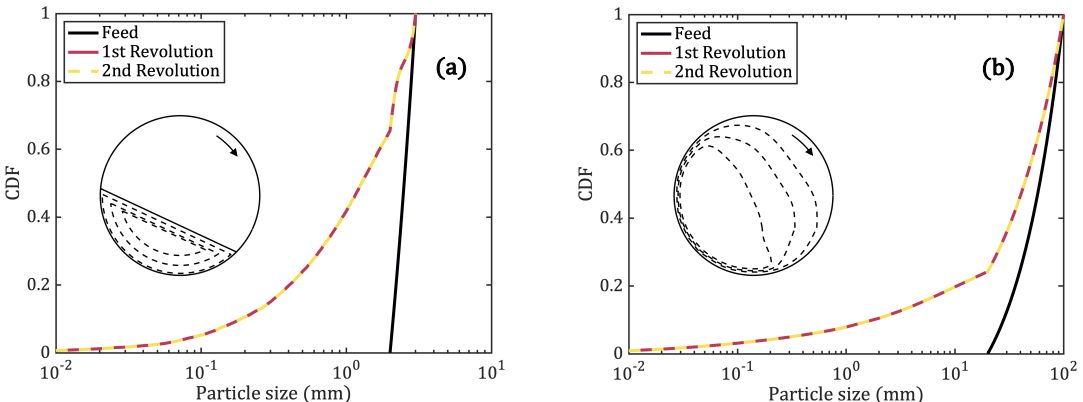


**Fig. 11:** Cumulative distribution function (CDF) of ultimate product particle sizes after one and two revolutions. (a) Ball mill, and (b) AG mill. This shows that when only the crushing mechanism is activated in the simulation, there is no significant crushing after one revolution of the mill. (As will be shown in Part II, this phenomenon disappears when considering further particle size dynamics through the mechanism of segregation and mixing).

due to impacts between the particles and therefore, the scaled mineral strength parameters in the simulation represent a weak crushable mineral.

For the AG mill simulation, we considered a mill with a diameter ( $d$ ) of 6 m rotating at 13.5 rpm, and the feed consisting of particles uniformly distributed between 20 mm - 100 mm in size. These operating parameters lie within the range that is typically associated with actual AG and SAG mills [43, 10]. The crushing strength

parameters for this simulation correspond to the mineral Feldspar and are based on single particle crushing tests by [44]. The fragment size distribution parameters are also for the mineral Feldspar derived from the single particle crushing results by [64]. The impact velocity parameters could be determined experimentally for the mineral chosen in this study. However, we rather estimate these parameters based on the impact crushing results

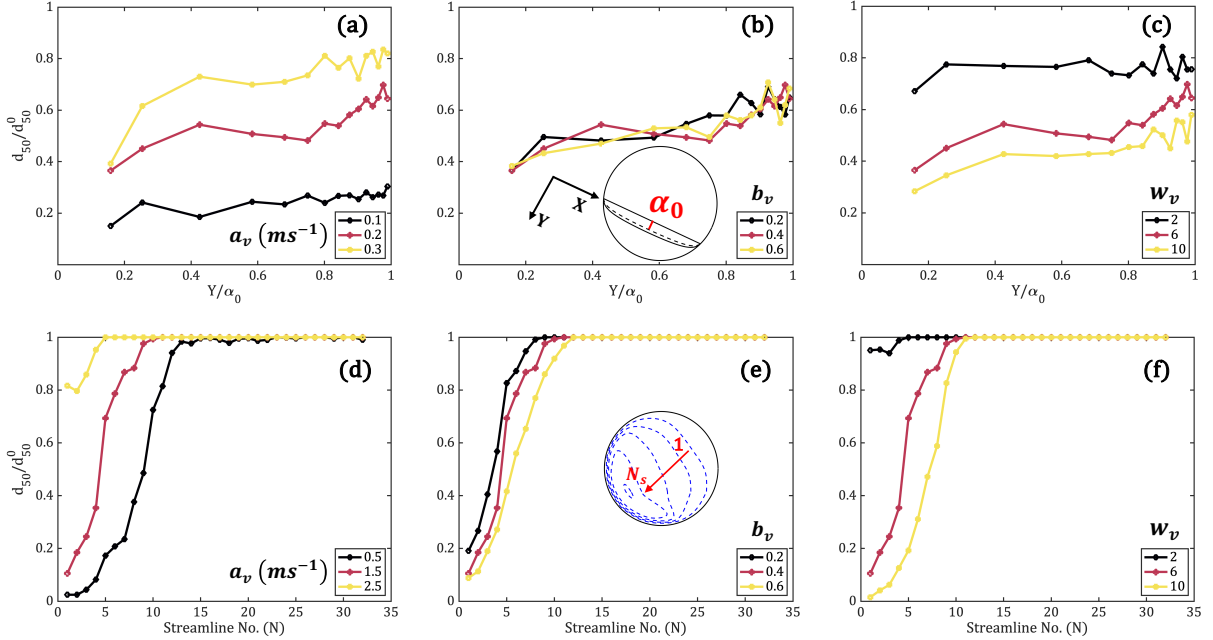


**Fig. 12:** Evolution of mean particle size ( $d_{50}$ ) normalized with respect to the feed mean particle size ( $d_{50}^0$ ) for variation in values of impact velocity parameters  $a_v$ ,  $b_v$  and  $w_v$ . The base values of the parameters are listed in Table 1. Only one of the parameters is varied at a time keeping the other two parameters equal to their base values. [Top - ball mill] The horizontal axis represents the depth of the flow measured from the free surface and normalised with respect to the maximum depth of zero velocity line ( $\alpha_0$ ). [Bottom - AG mill] The horizontal axis corresponds to the number of streamlines denoted from 1 to  $N_s$  as shown in the inset at the bottom figure e (colour figure online).

of [30] for cement-mortar balls. Here, our assumption is that these values would not differ much for the minerals. In order to check the sensitivity of these impact velocity parameters on crushing, we do a parametric study towards the end of this paper.

For the conceptual ball mill simulation, we utilised a mill of diameter( $d$ ) of 30 cm rotating at 6.3 rpm speed, and the feed consisted of particles with a uniform size distribution ranging between 2 mm - 3 mm. The value of the crushing strength parameter ( $\sigma^m$ ) was chosen to represent a weak, crushable mineral and its value is taken two orders of magnitude lower than the crushing strength of the mineral used in the AG mill simulations. Similarly, we also scale the impact velocity parameters for the ball mill based on the corresponding value obtained for the AG mill.

Given the parameters above, and the hierarchical streamline method, we can track the evolution of particle size at any point in space

and time inside the ball mill. Fig. 10a and 10b illustrate the cumulative distribution functions (CDFs) of particle size for different streamlines in the flow region after one revolution of the ball mill and the AG mill respectively.

The CDF plots provide clear insights into the influence of the fluctuating velocities on the crushing of particles in the granular flow. Notably, streamlines passing through regions of higher fluctuating velocity experience more crushing. In addition to generating CDF plots for individual streamlines, it is instructive to plot the overall or ultimate CDF that represents the entire material within each given mill, after one mill revolution. This product CDF is the weighted average by mass of the CDFs for each streamline, which is specified by

$$F_u(s) = \frac{1}{\mathcal{M}_{total}} \sum_{p=1}^{N_s} \sum_{q=1}^{N_p} F_{p,q}(s) \times \mathcal{M}_{p,q}, \quad (13)$$

where  $F_{p,q}(s)$  is the cumulative mass distribution function,  $\mathcal{M}_{p,q}$  is the mass of particles in a material point for a given streamline and  $\mathcal{M}_{total}$  is the total mass of particles in the system which can be calculated as

$$\mathcal{M}_{total} = \sum_{p=1}^{N_s} \sum_{q=1}^{N_p} \mathcal{M}_{p,q}. \quad (14)$$

The results of the ultimate CDF of the particle sizes are shown in Fig. 10a and 10b for the ball and the AG mills, respectively. These ultimate CDF plots give novel information about the overall extent of crushing in the mill at any given point in time.

Another significant finding from the simulations is that without segregation and mixing, no crushing could happen within the system after one revolution of the mill, as indicated by the CDF plots. Figs. 11a and 11b show the evolution of the CDF of the ultimate product particle sizes for the ball and AG mills, respectively. The CDFs do not evolve with any further rotation of the mill beyond one revolution. This behaviour is attributed to the current simulation setup, where the particles are only undergoing crushing without any mixing and segregation. As the particles crush, they attain a relatively stable configuration along the material points such that they are cushioned against further crushing. With the heterarchical stochastic physics of mixing and segregation (developed in Part II) not being activated at this stage, there is no mechanism that will disturb this cushioned state of particles after one revolution. However, with the introduction of mixing and segregation, as we will see in the next Part II of this work, the particles would no longer remain protected from further crushing after one mill revolution, allowing the particle size distribution to continuously evolve as the mill undergoes further revolutions.

The heterarchical model introduced in this study includes several parameters, namely  $a_v$ ,  $b_v$ , and  $w_v$ , which are dependent on the impact velocity (or fluctuating velocity) of particles. Here we provide a short demonstration of the effects of these parameters on the crushing simulations. In Figure 12, we illustrate the variation of the mean particle size ( $d_{50}$ ) with changes to these parameters for both the ball and the AG mills. It can be seen from the plots that for both the ball mill and the AG mill, the mean particle size varies

significantly with the variation of the parameters  $a_v$  and  $w_v$  while there is no significant change in mean particle size with variation of the parameter  $b_v$ . Overall, it can be concluded that the mean grain size increases with an increase in the value of parameter  $a_v$  while it decreases with an increase in the value of parameter  $w_v$ .

Lastly, we present the numerical robustness of the heterarchical model. This robustness is demonstrated by varying the number of cells ( $M$ ) along the microstructural coordinate ( $z$ ) and monitoring the resulting evolution of the product size for any streamline. As shown in Figure 13 for the AG mill simulation case, the results indicate that even with  $M = 10^2$ , meaning ten times fewer cells than what is used in the present study, we obtain stable results that are independent of the number of heterarchical cells. In addition to the numerical robustness, the results show that for a very high number of heterarchical cells, we get a smooth deterministic particle size distribution. This reaffirms the fact that the heterarchical model has a well-defined continuum limit as previously demonstrated by [33].

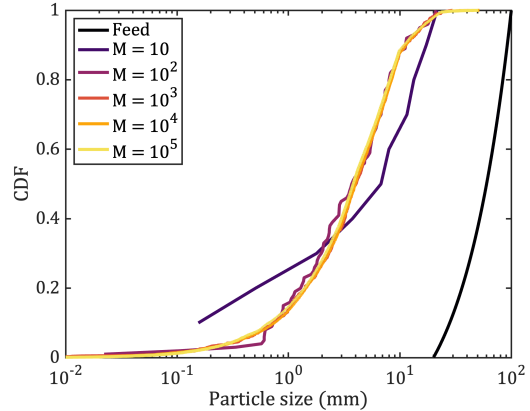


**Fig. 13:** Cumulative distribution function (CDF) of the product particle sizes for a streamline of the AG mill as a function of the number of cells ( $M$ ) along the heterarchical coordinate (colour figure online).

## 6 Discussion

We have introduced a new methodology to model industrial comminution, utilising the innovative

763 concept of heterarchical multiscale modelling com- 812  
764 bined with the streamline method. This work 813  
765 (Part I and II) serves as the foundational basis for 814  
766 the heterarchical comminution model, uncovering 815  
767 the particle size dynamics occurring inside rotary 816  
768 mills. However, at this stage, the model does not 817  
769 capture the entire particle size dynamics of the 818  
770 rotary mills. 819

771 This Part covers the particle size dynamics of 820  
772 kinetic crushing occurring due to impacts and the 821  
773 second Part covers the particle size dynamics of 822  
774 segregation and mixing. Other than impact crush- 823  
775 ing, there are other modes of particle breakage in 824  
776 rotary mills such as abrasion or attrition, chip- 825  
777 ping, and incremental breakage [15]. These modes 826  
778 of breakage are not incorporated yet into the het- 827  
779 erarchical model and require further investigation. 828

780 In addition to these particle size dynam- 829  
781 ics, further considerations remain to be explored 830  
782 for incorporation into the heterarchical model. 831  
783 Firstly, including grinding media into the mill 832  
784 charge, which plays a crucial role in particle crush- 833  
785 ing for ball and SAG mills. Secondly, addressing 834  
786 the input and output material flux. In actual mill 835  
787 operation, there is a continuous flux of material 836  
788 with finer particles exiting the mill from the dis- 837  
789 charge end and fresh feed material being fed from 838  
790 the other end. This rate of mass flux will influence  
791 the grinding of the material. Thirdly, considering 839  
792 the influence of water in the grinding operation. 840  
793 The water is expected to help reducing material 841  
794 friction while adding viscosity, maintain charge 842  
795 density, and control the discharge of fine materials 843  
796 through the mill. Lastly, considering the effect of 844  
797 lifter design on mill performance, and controlling 845  
798 the wear of lifters and grinding balls. These objec- 846  
799 tives form part of this ongoing project, and further 847  
800 developments will contribute to a more compre- 848  
801 hensive and versatile heterarchical comminution 849  
802 model for the mineral processing industry. 850

## 803 7 Conclusions

804 This study presents a new method based on 852  
805 stochastic heterarchical multiscale modelling for 853  
806 studying comminution in rotary mills. This new 854  
807 approach allows us to obtain the particle size dis- 855  
808 tribution at any point in space and time within the 856  
809 mill domain and it can deal with arbitrarily large 857  
810 numbers of particles, allowing us to accurately 858  
811 account for the polydispersity of particle sizes 859

in rotary mills. This method has a well-defined continuum limit as it gives smooth deterministic results for a large number of heterarchical cells.

The highlights of this paper are: Firstly, we derive the heterarchical rule governing the kinetic crushing of particles, which is predominant in rotary mills due to frequent particle collisions. Secondly, we build up the comminution model for rotary mills by integrating the concept of heterarchy and the streamline method.

Here, we uncover the physics of particle size dynamics occurring inside the mill with a focus exclusively on the crushing mechanism. The investigation of the other two important particle size mechanisms of mixing and segregation is reserved for Part II. Finally, We demonstrate the application of the heterarchical model in predicting the time evolution of particle size distribution for a ball mill and an AG mill.

Using this model, we want to empower operators with the ability to understand the effect of mill operating parameters such as degree of filling, mill speed, feed size distribution, and the fraction of grinding media in the mill charge. By providing this understanding the operator can decide on the optimum value of these parameters, leading to enhanced mill performance.

## Appendix A Analytical solution for velocity in ball mills

The analytic solution [22] for the bulk flow in ball mills is suitable for low rotational speeds in the so-called rolling flow regime ( $10^{-4} < F_r < 10^{-2}$ , with  $F_r$  being the Froude number [42]). The rolling flow regime [3, 21, 42] is characterized by a near levelled free surface inclined at the dynamic angle of repose ( $\varphi$ ) of the material. The flow can be divided into two distinct regions, *i.e.*, an active region and a passive region as shown in Fig 4a. The passive region occupies the bulk of the material. In this region, the particles move as a rigid body and are carried up along the ball mill with a velocity equal to the angular velocity of the mill. As the particles reach the free surface, they start to cascade down into the active region which is characterized by shear and volumetric deformations. The active region of the flow is where we would expect

most of the particle size dynamics from crushing, mixing, and segregation of particles to occur. The interface between the active and the passive region is defined by the  $\delta$ -profile. In the active region, the velocity is maximum at the free surface and it decreases along the depth of flow. The point where the velocity becomes zero is defined by the  $\alpha$ -profile.

The velocity solution is derived using the momentum and mass balance equations. Here, we present the solution for the velocity. The streamwise velocity (along the x-direction) in the active layer can be calculated as

$$u = u_s - \left[ \frac{1+\Lambda}{\Lambda} u_s - \frac{\Lambda}{1-\Lambda} \omega (H + \delta) \right] \left( \frac{y}{\delta} \right) + \left[ \frac{u_s}{\Lambda} - \frac{\omega(H+\delta)}{1-\Lambda} \right] \left( \frac{y}{\delta} \right)^2, \quad (\text{A.1})$$

where  $H$  is the depth of the free surface from the centre of the ball mill,  $\delta$  is the depth of the active-passive interface measured from the free surface,  $\omega$  is the angular velocity,  $u_s$  is the free surface velocity,  $\Lambda = \alpha/\delta < 1$  is the parameter defining the rheological properties of the flowing material, and  $\alpha$  is the depth measured from free surface to the point of zero streamwise velocity (see Fig. 4a).

The active-passive interface ( $\delta$ ) profile is given as

$$\delta = \left( - \left[ \frac{3\Lambda-1}{\Lambda} u_s + \frac{4-3\Lambda}{1-\Lambda} \omega H \right] + \sqrt{\left[ \frac{3\Lambda-1}{\Lambda} u_s + \frac{4-3\Lambda}{1-\Lambda} \omega H \right]^2 + \frac{12\omega^2(2Lx-x^2)}{1-\Lambda}} \right) / 2 \left( \frac{\omega}{1-\Lambda} \right), \quad (\text{A.2})$$

where we have used the parabolic free surface velocity profile given by [3]:

$$u_s = \frac{\omega L^2}{\alpha_0} \left[ 1 - \left( \frac{x-L}{L} \right)^2 \right], \quad (\text{A.3})$$

in which  $L$  is the half chord length of free surface and  $\alpha_0 = \alpha_{x=L}$

The transverse velocity (along the y-direction) is negligible [3] and is thus ignored. The passive region is typified by rigid body rotation, where the velocity can simply be calculated as

$$v = \omega(y + H). \quad (\text{A.4})$$

Fig. A1(a) shows the variation of the free surface velocity ( $u_s$ ) normalized with respect to the maximum free surface velocity ( $u_m$ ). The velocity variation along the depth at the centre of the flow is shown in Fig. A1(b). It can be seen from the figure that for the depth of the flow between  $y \geq \alpha$

and  $y < \delta$  in the active region, the mass moves along with the drum but the flow is not a rigid body motion.

## Appendix B DEM simulation for AG mill

The Discrete Element Method (DEM) simulations were carried out using the open source software Liggghts [37]. For simplicity and comparison with industrial conditions, the parameters of the simulation are given with dimensions in the following. A total of 45,000 particles are simulated with a uniform diameter distribution by number between 0.02 and 0.1 m, and density 2500 kg.m<sup>-3</sup>. The contact force between the particles follows a non-linear (hertzian) inelastic frictional law with Young's modulus of 0.5 GPa, Poisson's ratio of 0.3, restitution coefficient of 0.6, and friction coefficient of 0.5 [9]. The particles are integrated in time using a Verlet algorithm with timestep 10  $\mu$ s, low enough to ensure proper resolution of tracking collisions between particles.

The particles are placed in a cylindrical mill of diameter 6 m and length 2 m rotating around its horizontal axis at a speed of 13.5 rpm, leading to a typical Froude number of 1.4. The perimeter of the mill is lined with 40 lifters of height 10 cm to prevent slippage between the particles and the mill and to mimic industrial equipment. Contact properties between walls and particles are the same as between particles.

After the particles are inserted and the rotation started, the flow eventually reaches a steady state, from which all the particle properties (location, velocity, contact forces, etc.) are extracted every 0.01 s. This avoids correlation between the different snapshots of the simulation and allows to perform time averaging. The spatial averaging is performed using the coarse-graining method indicated in [63], by specifically following the implementation detailed in [31]. The fields are calculated on a grid in space using a Lucy function as the coarse-graining window  $w$ , with a width  $c = 0.4$  m:

$$w(x) = \frac{105}{16\pi c^3} \left( -3 \left( \frac{x}{c} \right)^4 + 8 \left( \frac{x}{c} \right)^3 - 6 \left( \frac{x}{c} \right)^2 + 1 \right) \mathcal{H}(c - x). \quad (\text{B.1})$$

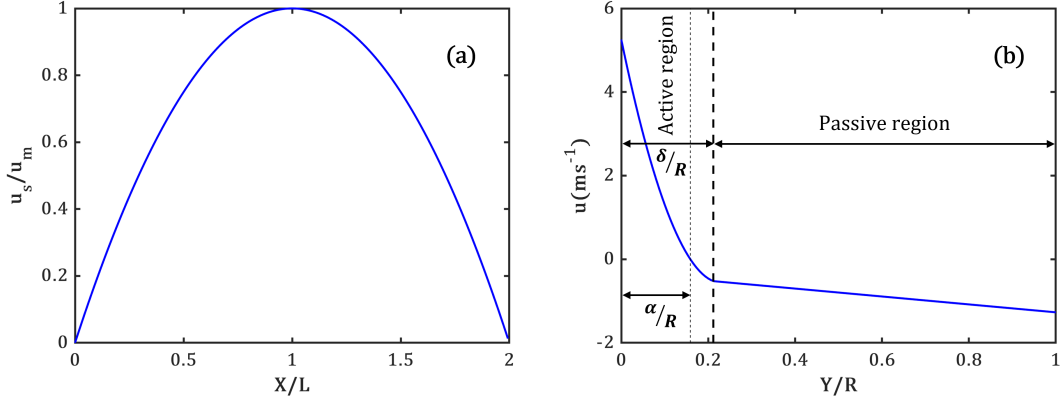


**Fig. A1:** Velocity distribution obtained using the analytical solution of Ding et al. [22]. (a) Free surface velocity normalized with respect to its maximum value, and (b) Velocity variation along the depth as measured at the midpoint of the free surface.

The bulk density  $\rho_b$  and velocity  $\mathbf{v}$  fields are obtained using:

$$\rho_b(\mathbf{x}) = \sum_i m_i w(|\mathbf{x} - \mathbf{x}_i|) \quad (\text{B.2})$$

$$\rho_b \mathbf{v}(\mathbf{x}) = \sum_i m_i \mathbf{v}_i w(|\mathbf{x} - \mathbf{x}_i|) \quad (\text{B.3})$$

where  $\mathbf{x}_i$ ,  $\mathbf{v}_i$ ,  $m_i$  are the position, velocity, and mass of particle  $i$ , respectively, and  $\mathbf{x}$  is the position at which the field is estimated. The velocity field is then time-averaged to obtain  $\langle \mathbf{v} \rangle$ , and the spatial gradients are taken to obtain the strain-rate tensor  $\dot{\epsilon} = \frac{1}{2}(\nabla \langle \mathbf{v} \rangle + \nabla^T \langle \mathbf{v} \rangle)$ . The volumetric strain rate is then calculated with  $\dot{\epsilon}_v = \text{Tr } \dot{\epsilon}$ , and we define the shear strain rate as  $\dot{\epsilon}_s = \sqrt{(\dot{\epsilon} - \frac{\dot{\epsilon}_v}{3}\mathbb{1}) : (\dot{\epsilon} - \frac{\dot{\epsilon}_v}{3}\mathbb{1})}$ , with  $\mathbb{1}$  the identity tensor.

The fluctuating velocity  $\mathbf{v}'$  is obtained using

$$\rho_b \mathbf{v}' = \sum_i m_i (\mathbf{v}_i - \langle \mathbf{v}(\mathbf{x}_i) \rangle) w(|\mathbf{x} - \mathbf{x}_i|), \quad (\text{B.4})$$

where  $\langle \mathbf{v} \rangle$  is linearly interpolated at the location of particle  $i$  from the field calculated at discrete grid points.

Finally, the static pressure  $P_s = \text{Tr } \boldsymbol{\sigma}$  is calculated from the contact forces  $\mathbf{f}_{ij}$  between particles  $i$  and  $j$  by

$$\boldsymbol{\sigma} = \sum_{\text{contacts}} \mathbf{f}_{ij} \otimes (\mathbf{x}_j - \mathbf{x}_i) \int_0^1 w(|\mathbf{x}_i + s(\mathbf{x}_j - \mathbf{x}_i)|) ds, \quad (\text{B.5})$$

with the integration performed numerically.

**Acknowledgments.** The authors would like to thank Molycop and The University of Sydney for financially supporting this project.

**Declaration of interests.** The authors did not receive support from any organization for the submitted work. No funding was received to assist with the preparation of this manuscript. No funding was received for conducting this study. No funds, grants, or other support was received.

## References

- [1] Narendra Ahuja. “Dot pattern processing using Voronoi neighborhoods”. In: *IEEE Transactions on Pattern Analysis and Machine Intelligence* 3 (1982), pp. 336–343.
- [2] Ebrahim Alaei, Beny Marks, and Itai Einav. “A hydrodynamic-plastic formulation for modelling sand using a minimal set of parameters”. In: *Journal of the Mechanics and Physics of Solids* 151 (2021), p. 104388.
- [3] Ebrahim Alizadeh et al. “Characterization of mixing and size segregation in a rotating drum by a particle tracking method”. In: *AIChE Journal* 59.6 (2013), pp. 1894–1905.
- [4] José E Andrade and Xuxin Tu. “Multiscale framework for behavior prediction in granular media”. In: *Mechanics of Materials* 41.6 (2009), pp. 652–669.
- [5] Mohsen M Baligh. “Strain path method”. In: *Journal of Geotechnical Engineering* 111.9 (1985), pp. 1108–1136.

- 958 [6] GR Ballantyne and MS Powell. “Bench- 1009  
 959 marking comminution energy consumption 1010  
 960 for the processing of copper and gold ores”. 1011  
 961 In: *Minerals Engineering* 65 (2014), pp. 109– 1012  
 962 114. 1013
- 963 [7] Perry Bartelt and Brian W McArdell. 1014  
 964 “Granulometric investigations of snow 1015  
 965 avalanches”. In: *Journal of Glaciology* 1016  
 966 55.193 (2009), pp. 829–833. 1017
- 967 [8] Mukesh Singh Bisht and Arghya Das. “DEM 1018  
 968 Study on Particle Shape Evolution dur- 1019  
 969 ing Crushing of Granular Materials”. In: 1020  
 970 *International Journal of Geomechanics* 21.7 1021  
 971 (2021), p. 04021101. 1022
- 972 [9] Nikolai V Brilliantov et al. “Model for colli- 1023  
 973 sions in granular gases”. In: *Physical review* 1024  
 974 E 53.5 (1996), p. 5382. 1025
- 975 [10] Marcos Bueno et al. “The dominance of 1026  
 976 the competent”. In: *Fifth International* 1027  
 977 *Autogenous and Semiautogenous Grinding* 1028  
 978 *Technology, University of British Columbia,* 1029  
 979 *Department of Mining and Mineral Process* 1030  
 980 *Engineering, Vancouver* (2011). 1031
- 981 [11] MP Bueno et al. “Multi-component 1032  
 982 AG/SAG mill model”. In: *Minerals* 1033  
 983 *Engineering* 43 (2013), pp. 12–21. 1034
- 984 [12] Rodrigo Carvalho and L Tavares. “A mech- 1035  
 985 anistic model of SAG mills”. In: *Proceedings* 1036  
 986 *of the IMPC* (2014). 1037
- 987 [13] YS Cheong et al. “Modelling fragment size 1038  
 988 distribution using two-parameter Weibull 1039  
 989 equation”. In: *International Journal of Min- 1040  
 990 eral Processing* 74 (2004), S227–S237. 1041
- 991 [14] Paul Cleary. “Modelling comminution 1042  
 992 devices using DEM”. In: *International Jour- 1043  
 993 nal for numerical and analytical methods in 1044  
 994 geomechanics* 25.1 (2001), pp. 83–105. 1045
- 995 [15] Paul W Cleary and RD Morrison. “Com- 1046  
 996 minution mechanisms, particle shape evo- 1047  
 997 lution and collision energy partitioning in 1048  
 998 tumbling mills”. In: *Minerals Engineering* 1049  
 999 86 (2016), pp. 75–95. 1050
- 1000 [16] Paul W Cleary and Rob D Morrison. “Pre- 1051  
 1001 diction of 3D slurry flow within the grinding 1052  
 1002 chamber and discharge from a pilot scale 1053  
 1003 SAG mill”. In: *Minerals Engineering* 39 1054  
 1004 (2012), pp. 184–195. 1055
- 1005 [17] Paul W Cleary, Rob D Morrison, and Matt 1056  
 1006 D Sinnott. “Prediction of slurry grinding 1057  
 1007 due to media and coarse rock interactions in 1058  
 1008 a 3D pilot SAG mill using a coupled DEM+ 1059
- SPH model”. In: *Minerals Engineering* 159 (2020), p. 106614.
- [18] Paul W Cleary, Rob Morisson, and Steve Morrell. “Comparison of DEM and experiment for a scale model SAG mill”. In: *International Journal of Mineral Processing* 68.1-4 (2003), pp. 129–165.
- [19] Claude Cunningham. “The Kuz-Ram Model for production of fragmentation from blasting”. In: *Proc. 1<sup>st</sup> Symp. on Rock Fragmentation by Blasting, Lulea*. 1983.
- [20] Frédéric Da Cruz et al. “Rheophysics of dense granular materials: Discrete simulation of plane shear flows”. In: *Physical Review E* 72.2 (2005), p. 021309.
- [21] YL Ding et al. “Granular motion in rotating drums: bed turnover time and slumping–rolling transition”. In: *Powder Technology* 124.1-2 (2002), pp. 18–27.
- [22] YL Ding et al. “Segregation of granular flow in the transverse plane of a rolling mode rotating drum”. In: *International Journal of Multiphase Flow* 28.4 (2002), pp. 635–663.
- [23] SA Dunning. “The grain size distribution of rock-avalanche deposits in valley-confined settings”. In: *Italian Journal of Engineering Geology and Environment* 1 (2006), pp. 117–121.
- [24] Itai Einav and Mark F Randolph. “Combining upper bound and strain path methods for evaluating penetration resistance”. In: *International journal for numerical methods in engineering* 63.14 (2005), pp. 1991–2016.
- [25] Gerald Farin, Josef Hoschek, and M-S Kim. *Handbook of computer aided geometric design*. Elsevier, 2002.
- [26] DW Fuerstenau and A-ZM Abouzeid. “The energy efficiency of ball milling in comminution”. In: *International Journal of Mineral Processing* 67.1-4 (2002), pp. 161–185.
- [27] Kurt D Gerdes et al. “The US Department of Energy–Office of Environmental Management’s International Program”. In: *Waste Management* 7 (2007).
- [28] Isaac Goldhirsch. “Stress, stress asymmetry and couple stress: from discrete particles to continuous fields”. In: *Granular Matter* 12.3 (2010), pp. 239–252.
- [29] Indresan Govender. “Granular flows in rotating drums: A rheological perspective”.

- 1059 In: *Minerals Engineering* 92 (2016), pp. 168–<sup>1109</sup>  
 1060 175.<sup>1110</sup>
- 1061 [30] Davide Ettore Guccione et al. “Predict-<sup>1111</sup>  
 1062 ing the fragmentation survival probability<sup>1112</sup>  
 1063 of brittle spheres upon impact from sta-<sup>1113</sup>  
 1064 tistical distribution of material properties”.<sup>1114</sup>  
 1065 In: *International Journal of Rock Mechanics*<sup>1115</sup>  
 1066 and *Mining Sciences* 142 (2021), p. 104768.<sup>1116</sup>
- 1067 [31] François Guillard and Benjy Marks. “Fric-<sup>1117</sup>  
 1068 tional hyperspheres in hyperspace”. In:<sup>1118</sup>  
 1069 *Physical Review E* 103.5 (2021), p. 052901.<sup>1119</sup>
- 1070 [32] Ning Guo and Jidong Zhao. “A coupled<sup>1120</sup>  
 1071 FEM/DEM approach for hierarchical mul-<sup>1121</sup>  
 1072 tiscale modelling of granular media”. In:<sup>1122</sup>  
 1073 *International Journal for Numerical Meth-<sup>1123</sup>*  
 1074 *ods in Engineering* 99.11 (2014), pp. 789–<sup>1124</sup>  
 1075 818.<sup>1125</sup>
- 1076 [33] Eric Huang, Benjy Marks, and Itai Einav.<sup>1126</sup>  
 1077 “Continuum homogenisation of stochastic<sup>1127</sup>  
 1078 comminution with grainsize fabric”. In:<sup>1128</sup>  
 1079 *Journal of the Mechanics and Physics of<sup>1129</sup>*  
 1080 *Solids* 138 (2020), p. 103897.<sup>1130</sup>
- 1081 [34] Kevin J. Hanley and Catherine O’Sullivan.<sup>1131</sup>  
 1082 “Analytical study of the accuracy of dis-<sup>1132</sup>  
 1083 crete element simulations”. In: *International<sup>1133</sup>*  
 1084 *Journal for Numerical Methods in Engineer-<sup>1134</sup>*  
 1085 *ing* 109.1 (2017), pp. 29–51.<sup>1135</sup>
- 1086 [35] Nitin Jain, Julio M Ottino, and Richard<sup>1136</sup>  
 1087 M Lueptow. “An experimental study of the<sup>1137</sup>  
 1088 flowing granular layer in a rotating tum-<sup>1138</sup>  
 1089 bler”. In: *Physics of Fluids* 14.2 (2002),<sup>1139</sup>  
 1090 pp. 572–582.<sup>1140</sup>
- 1091 [36] Jack Jeswiet and Alex Szekeres. “Energy<sup>1141</sup>  
 1092 consumption in mining comminution”. In:<sup>1142</sup>  
 1093 *Procedia CIRP* 48 (2016), pp. 140–145.<sup>1143</sup>
- 1094 [37] Christoph Kloss et al. “Models, Algorithms<sup>1144</sup>  
 1095 and Validation for Opensource DEM and<sup>1145</sup>  
 1096 CFD-DEM”. In: *Progress in Computational<sup>1146</sup>*  
 1097 *Fluid Dynamics, an International Journal*<sup>1147</sup>  
 1098 12.2–3 (2012), pp. 140–152.<sup>1148</sup>
- 1099 [38] Gang Ma et al. “Combined FEM/DEM<sup>1149</sup>  
 1100 modeling of triaxial compression tests for<sup>1150</sup>  
 1101 rockfills with polyhedral particles”. In:<sup>1151</sup>  
 1102 *International Journal of Geomechanics* 14.4<sup>1152</sup>  
 1103 (2014), p. 04014014.<sup>1153</sup>
- 1104 [39] Zvonimir Maranic et al. “A granular ther-<sup>1154</sup>  
 1105 mometer”. In: *Granular Matter* 23.2 (2021),<sup>1155</sup>  
 1106 pp. 1–15.<sup>1156</sup>
- 1107 [40] Benjy Marks and Itai Einav. “A heterarchi-<sup>1157</sup>  
 1108 cal multiscale model for granular materials<sup>1158</sup>  
 1109
- 1110 with evolving grainsize distribution”. In:  
 1111 *Granular Matter* 19.3 (2017), pp. 1–15.
- [41] GR McDowell and A Amon. “The application  
 1112 of Weibull statistics to the fracture of  
 1113 soil particles”. In: *Soils and foundations* 40.5  
 1114 (2000), pp. 133–141.
- [42] Jochen Mellmann. “The transverse motion  
 1115 of solids in rotating cylinders—forms of  
 1116 motion and transition behavior”. In: *Powder  
 1117 technology* 118.3 (2001), pp. 251–270.
- [43] S Mwansa, P Condori, and MS Powell.  
 1118 “Charge segregation and slurry transport  
 1119 in long SAG mills”. In: *Proceedings of  
 1120 the XXIII International Mineral Processing  
 1121 Congress (IMPC 2006) Promed Advertising  
 1122 Istanbul, Turkey*. 2006, pp. 81–86.
- [44] AFL Nakata et al. “A probabilistic approach  
 1123 to sand particle crushing in the triaxial  
 1124 test”. In: *Géotechnique* 49.5 (1999), pp. 567–  
 1125 583.
- [45] Yukio Nakata et al. “One-dimensional com-  
 1126 pression behaviour of uniformly graded  
 1127 sand related to single particle crushing  
 1128 strength”. In: *Soils and foundations* 41.2  
 1129 (2001), pp. 39–51.
- [46] Michał Nitka et al. “Two-scale modeling of  
 1130 granular materials: a DEM-FEM approach”.  
 1131 In: *Granular Matter* 13.3 (2011), pp. 277–  
 1132 281.
- [47] HR Norouzi, R Zarghami, and N Mostoufi.  
 1133 “Insights into the granular flow in rotating  
 1134 drums”. In: *Chemical Engineering Research  
 1135 and Design* 102 (2015), pp. 12–25.
- [48] Finn Ouchterlony. “The Swebrec© func-  
 1136 tion: linking fragmentation by blasting and  
 1137 crushing”. In: *Mining Technology* 114.1  
 1138 (2005), pp. 29–44.
- [49] DJ Parker et al. “Positron emission  
 1139 particle tracking—a technique for studying  
 1140 flow within engineering equipment”.  
 1141 In: *Nuclear Instruments and Methods in  
 1142 Physics Research Section A: Accelerators,  
 1143 Spectrometers, Detectors and Associated  
 1144 Equipment* 326.3 (1993), pp. 592–607.
- [50] Christopher J Phillips and Timothy RH  
 1145 Davies. “Determining rheological parame-  
 1146 ters of debris flow material”. In: *Geomor-  
 1147 phology* 4.2 (1991), pp. 101–110.
- [51] N Pollet and J-LM Schneider. “Dynamic dis-  
 1148 integration processes accompanying trans-  
 1149 port of the Holocene Flims sturzstrom

- 1160 (Swiss Alps)”. In: *Earth and Planetary Sci-*<sub>1210</sub>  
 1161 *ence Letters* 221.1-4 (2004), pp. 433–448. <sub>1211</sub>
- 1162 [52] GK Reynolds et al. “Breakage in granula-<sub>1212</sub>  
 1163 tion: A review”. In: *Chemical Engineering*<sub>1213</sub>  
 1164 *Science* 60.14 (2005), pp. 3969–3992. <sub>1214</sub>
- 1165 [53] Yevgeny Rozenblat et al. “Impact<sub>1215</sub>  
 1166 velocity and compression force relation-<sub>1216</sub>  
 1167 ship—Equivalence function”. In: *Powder*<sub>1217</sub>  
 1168 *technology* 235 (2013), pp. 756–763. <sub>1218</sub>
- 1169 [54] Yevgeny Rozenblat et al. “Selection and<sub>1219</sub>  
 1170 breakage functions of particles under impact<sub>1220</sub>  
 1171 loads”. In: *Chemical Engineering Science* 71<sub>1221</sub>  
 1172 (2012), pp. 56–66. <sub>1222</sub>
- 1173 [55] DA Santos et al. “A hydrodynamic analysis<sub>1223</sub>  
 1174 of a rotating drum operating in the rolling<sub>1224</sub>  
 1175 regime”. In: *Chemical Engineering Research*<sub>1225</sub>  
 1176 *and Design* 94 (2015), pp. 204–212. <sub>1226</sub>
- 1177 [56] Jürgen Tomas et al. “Impact crushing of<sub>1227</sub>  
 1178 concrete for liberation and recycling”. In:  
 1179 *Powder Technology* 105.1-3 (1999), pp. 39–  
 1180 51.
- 1181 [57] D Tromans and JA Meech. “Fracture tough-  
 1182 ness and surface energies of covalent min-  
 1183 erals: theoretical estimates”. In: *Minerals*  
 1184 *engineering* 17.1 (2004), pp. 1–15.
- 1185 [58] D Tromans and JA Meech. “Fracture tough-  
 1186 ness and surface energies of minerals: theo-  
 1187 retical estimates for oxides, sulphides, sili-  
 1188 cates and halides”. In: *Minerals Engineering*  
 1189 15.12 (2002), pp. 1027–1041.
- 1190 [59] Yu Wang et al. “A coupled FEM-DEM  
 1191 study on mechanical behaviors of gran-  
 1192 ular soils considering particle breakage”.  
 1193 In: *Computers and Geotechnics* 160 (2023),  
 1194 p. 105529.
- 1195 [60] DM Weedon and F Wilson. “Modelling iron  
 1196 ore degradation using a twin pendulum  
 1197 breakage device”. In: *International Journal*  
 1198 *of Mineral Processing* 59.3 (2000), pp. 195–  
 1199 213.
- 1200 [61] Nirmal S Weerasekara et al. “The contribu-  
 1201 tion of DEM to the science of comminution”.  
 1202 In: *Powder technology* 248 (2013), pp. 3–24.
- 1203 [62] Waloddi Weibull et al. “A statistical distri-  
 1204 bution function of wide applicability”. In:  
 1205 *Journal of applied mechanics* 18.3 (1951),  
 1206 pp. 293–297.
- 1207 [63] Thomas Weinhart et al. “Coarse-grained  
 1208 local and objective continuum description  
 1209 of three-dimensional granular flows down an
- 1210 inclined surface”. In: *Physics of fluids* 25.7  
 1211 (2013).
- 1212 [64] Saburo Yashima, Shoichi Morohashi, and  
 1213 Fumio Saito. “Single particle crushing under  
 1214 slow rate of loading”. In: *Science Reports of*  
 1215 *the Research Institutes, Tohoku University*  
 1216 *Ser A, Physics, Chemistry And Metallurgy*  
 1217 28 (1979), pp. 116–133.
- 1218 [65] Ping Yu et al. “Development of a dynamic  
 1219 mill model structure for tumbling mills”.  
 1220 In: *XXVII International Mineral Processing*  
 1221 *Congress-IMPC 2014 Conference Proceed-  
 1222 ings, Gecamin Digital Publications Santia-  
 1223 go, Chile*. 2014, pp. 41–51.
- 1224 [66] Qian Zhou, Wen-Jie Xu, and Retief Lubbe.  
 1225 “Multi-scale mechanics of sand based on  
 1226 FEM-DEM coupling method”. In: *Powder*  
 1227 *Technology* 380 (2021), pp. 394–407.